JOURNAL OF SOLID STATE CHEMISTRY 137, 231–241 (1998)
ARTICLE NO. SC977711

Kinetics and Mechanism of Prephase State Accumulation and Phase Transition in Crystals of 2-Bromo-2-Nitropropane-1,3-Diol

N. I. Golovina, A. V. Raevskii, B. S. Fedorov, I. G. Gusakovskaya, R. F. Trofimova, and L. O. Atovmyan

Institute of Chemical Physics in Chernogolovka, Russian Academy of Sciences, Chernogolovka, 142432, Russia

Received July 14, 1997; in revised form November 12, 1997; accepted November 24, 1997

The structure of two phases of 2-bromo-2-nitropropane-1,3-diol (1,2) synthesized by two different methods has been investigated. Calorimetric measurements of temperature behavior of crystals I and II have been conducted, with the crystals manifesting phase transition in a wide temperature range, 193–343 K. The changes of the initial monoclinic phase I featuring the "prephase" state have been studied during heating to the phase transition temperature for polycrystal samples. X-ray patterns showing that polycrystal I transformed into a final cubic phase at 375 K have been identified. The phase transition process in separate crystals of 2-bromo-2-nitropropane-1,3-diol has been investigated in a special hot stage under an optical microscope. The kinetic parameters of the prephase accumulation have been calculated from kinetic measurement of the reflection intensities (110), (200), and (040) of monoclinic phase I at temperatures 348, 358, and 363 K.

INTRODUCTION

At present the processes accompanying phase transition should probably be considered as phenomena proceeding in an extended space zone of external parameters (3, 4). In particular, this consideration relates to crystal structures formed by interaction forces of a dissimilar nature (ionic, molecular, H-bond, exchange cooperation, and so on (5)). The forces forming the interaction depend differently on external impact. For instance, the temperature variations in the crystal structures before the phase transition point must lead to structural changes preparing a real phase transition and converting the structure to a prephase state. The above-mentioned situation relates first of all to nitrocompounds, which have a comparatively low-energy crystal structure and a low barrier for conversion of molecules. The experimental methods for studying such phenomena have to be sufficiently "gentle" and at the same time very selective to trace small changes both in individual molecules and in the crystal structure as a whole. X-ray analysis and spectral techniques can be singled out first of all for studying the behavior of these compounds under various external conditions (temperature, for example).

An investigation of changes in the crystal lattice of 2-bromo-2-nitropropane-1,3-diol occurring in the initial structure during preparation for phase transition from a monoclinic to a cubic phase is presented in this paper. In previous work (6), the authors have studied the behavior of 2,4,6-trinitrotoluene and benzotrifuroxane in a prephase state.

EXPERIMENTAL

The choice of 2-bromo-2-nitropropane-1,3-diol was not accidental. The synthesis of the compound (1) and its molecular and crystal structure have been investigated earlier (7). It is also known that the crystals of 2-bromo-2-nitropropane-1,3-diol enter a randomized state. We have repeated the synthesis (1) based on a sodium salt of 2-bromo-2-nitropropane-1,3-diol and molecular bromine,

$$Na\cdot O_2N=C(CH_2OH)_2 \xrightarrow[-NaBr]{Br} BrC(NO_2)(CH_2OH)_2 \quad (\mathbf{I})$$

and have also repeated an X-ray analysis of the separated crystals (7). While studying chemical conversions of a 2-nitroethanol sodium salt in aqueous ammonia, we succeeded in separating and identifying previously unknown compound—a sodium salt of 2-oxo-3-hydroxypropionic acid oxime (2),

$$2HOCH_2CH{=}N\begin{matrix}\nearrow O\\ \searrow \bar{O}\end{matrix} Na^+ \xrightarrow{NH_3,H_2O} \begin{matrix}NOH\\ \|\\ HOCH_2C{-}COONa\cdot 2H_2O\end{matrix} \quad (\mathbf{III}).$$

The compound 2-bromo-2-nitropropane-1,3-diol with a previously unknown conformation has been prepared through

0022-4596/98 $25.00

bromination of salt III,

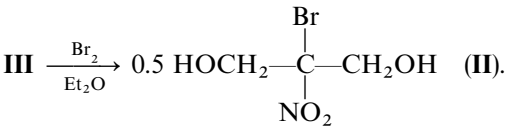

1. X-ray Diffraction Study

The structures of two phases of crystals of 2-bromo-2-nitropropropane-1,3-diol (**I**, **II**) and sodium salt of 2-oxo-3-hydroxypropionic acid oxime (**III**) have been investigated. Crystallographic data are presented in Table 1.

The intensities of reflections were measured in the range $0.02 \leq \sin\Theta/\lambda \leq 0.5$ on a four-circle KM-4 (KUMA-Diffraction, Poland) diffractometer using the $\omega/2\Theta$ scanning technique. Structures of **I**, **II**, and **III** were solved by the direct method using the SHELX-86 program package on a personal computer. Atomic coordinates in the structures of **I**, **II**, and **III** were refined by the full-matrix least squares method using anisotropic thermal parameters for nonhydrogen atoms and isotropic thermal parameters for hydrogen atoms. Atomic coordinates of hydrogen atoms were located from the difference electron density synthesis. The phases **I** and **II**, synthesized from different parent compounds, were crystallized in the same space group, *Cc*, with dissimilar unit cell parameters and crystal densities. As is shown in Figs. 1 and 2, an identical molecular package is characteristic of the **I** and **II** structures with the exception of OH groups. At the same time, one can see from Fig. 3 that the molecular conformations differ. The C–O and C–C bonds in molecule **I** are in the antiperiplanar position, while in molecule **II** they are synclinal. The Newman projections for molecules **I** and **II** are shown in Fig. 4. The differences indicated manifest in the values of the torsion angles: O(2)–C(3)–C(2)–C(1) and O(1)–C(1)–C(2)–C(3) in molecule **I** are 174.5° and 167.5°, respectively, while in molecule **II** the torsion angles O(1)–C(1)–C(2)–C(3) and O(2)–C(3)–C(2)–C(1) are 48.2° and 54.6°, respectively. Such conformational dissimilarity in the constitution of the very same chemical compound prepared

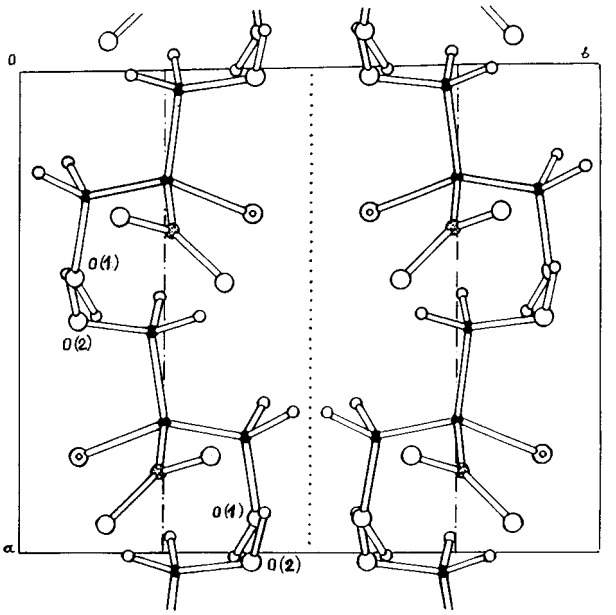

FIG. 1. Projection of the structure **I** on plane *ab*.

TABLE 1
Crystallographic Data of the Structures I—$C_3H_6BrNO_4$, II—$C_3H_6BrNO_4$, and III—$NaC_3H_4NO_4 \cdot 2H_2O$

	Structure		
Lattice parameters	**I**	**II**	**III**
a (Å)	8.027(3)	8.053(3)	9.086(3)
b (Å)	9.661(3)	9.676(3)	6.305(2)
c (Å)	8.963(3)	8.989(3)	6.839(2)
α (°)	90.00	90.00	104.49(2)
β (°)	91.01(2)	90.88(2)	99.40(2)
γ (°)	90.00	90.00	77.46(2)
V (Å^3)	695.0(6)	700.7(5)	367.8(2)
d_{calc} (g/cm^3)	1.910(3)	1.895(2)	1.598(2)
Space group	*Cc*	*Cc*	$P\bar{1}$
z	4	4	2
λ(A)	0.7092	0.7092	0.7092
Mu (mm^{-1})	5.86	5.86	0.200
M	200.0	200.0	177.1
Number reflection	659	585	1100
R	0.048	0.059	0.062

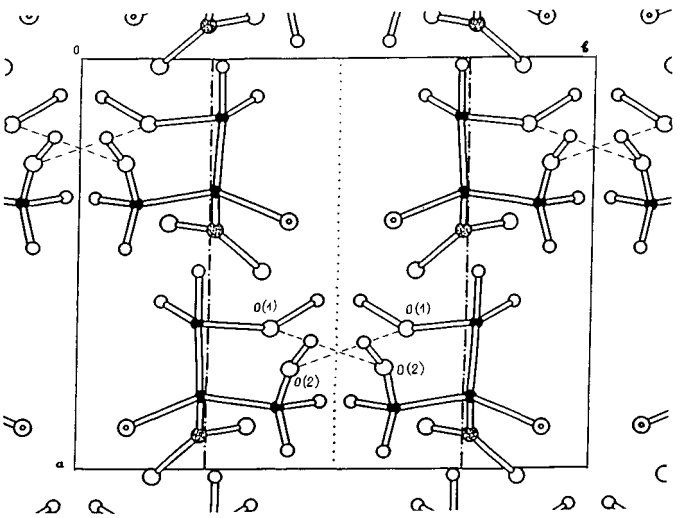

FIG. 2. Projection of the structure **II** on plane *ab*.

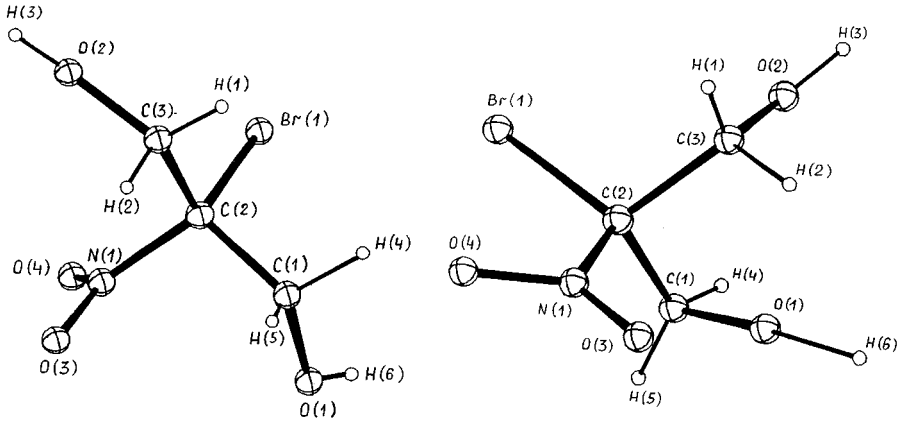

FIG. 3. Conformation of the molecules **I** and **II**.

from different parent compounds might be explained entirely by particularities of the parent compound **III**. That is why we have conducted an X-ray study of crystal **III**. The conformation of anion **III** (Fig. 5) testifies for charge delocalization about the flat anion fragment in which the atoms O(1), O(2), C(1), C(2), C(3), and N(1) are placed practically in one plane: torsion angles O(1)–C(1)–C(2)–C(3), O(1)–C(1)–C(2)–N(1), O(2)–C(1)–C(2)–C(3), and O(2)–C(1)–C(2)–N(1) are 5.3°, 176.2°, 176.2°, and 2.3°, while torsion angles O(3)–C(3)–C(2)–N(1) and O(3)–C(3)–C(2)–C(1) amount to 40.5° and 137.9°, respectively. The atomic coordinates of the structures **I**, **II**, **III** are given in Tables 2, 3, and 4.

As follows from the experimental data, the conformation of molecule **II** can be considered to be built into the conformation of the $=C–CH_2OH$ fragment of anion **III** and conserved until the moment of isolation of molecule **II**. In turn, the conformational differences in the positions of the OH groups in molecules **I** and **II** create different architectures of the H-bonds in the crystals of these conformers. The distance between the oxygen atoms of the neighboring molecules O(1) ⋯ O(2) is 2.712 Å in molecule **I**, while the same distance in the structure of **II** is 3.044 Å. In both cases, the H-bonds form indefinite chains: in structure **I** the chain is generated by the *n* plane, in structure **II** by the *c* plane (Figs. 1 and 2).

Calculation of the energy for the two structures by the atom–atom potential method shows that the crystal structure of **I** is 4.24 kcal · mol^{-1} more favorable than that of **II** including the contribution of the H-bonds (1.66 kcal · mol^{-1}). The total energy of structure **I** amounts to about 16 kcal · mol^{-1}, the energy of hydrogen bonds to about 6 kcal · mol^{-1}. According to the SCF MO/STO-3G calculations, the overall electron energy of both molecules **I** and **II** is essentially the same; calculations of the strain energy for the two conformations give different values. The conformation of molecule **II** is more favourable than that of **I** by 1.5 kcal · mol^{-1}. Thus, the unfavorable conformation of **I** is compensated for by a gain in the energy of the H-bonds in the crystal.

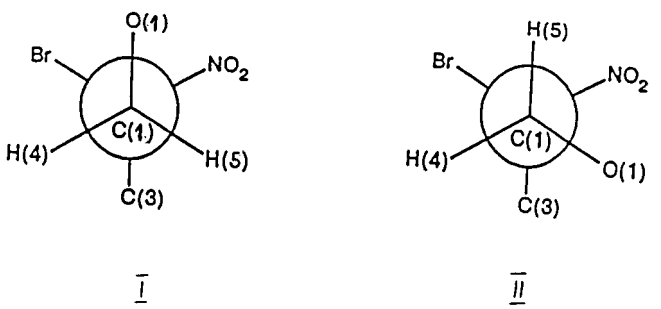

FIG. 4. Newman projection of the molecules **I** and **II**.

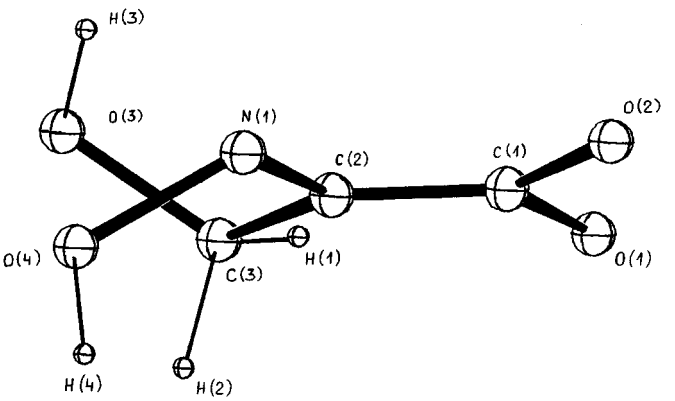

FIG. 5. Conformation and anion of the structure **III**.

TABLE 2
Atomic Coordinates ($\times 10^4$) in the Structure I

Atom	*X*	*Y*	*Z*
Br(1)	1961(1)	9002(2)	2774(2)
O(1)	642(19)	5834(13)	3298(18)
O(2)	4801(21)	8952(14)	5349(16)
O(3)	638(29)	8492(23)	5685(25)
O(4)	1993(27)	6728(21)	6420(16)
N(1)	1687(21)	7618(19)	5513(21)
C(1)	2373(78)	6098(40)	3453(50)
C(2)	2717(22)	7527(16)	4098(16)
C(3)	4521(27)	7719(21)	4525(28)

TABLE 4
Atomic Coordinates ($\times 10^4$) in the Structure III

Atom	*X*	*Y*	*Z*
Na(1)	9272(2)	972(3)	7598(3)
O(1)	3766(4)	8082(5)	7977(6)
O(2)	2766(3)	4965(5)	6676(5)
O(3)	7970(3)	4675(6)	7182(6)
O(4)	6803(4)	1130(5)	8167(7)
O(5)	10220(4)	− 2520(7)	8652(6)
O(6)	11512(4)	857(6)	6141(6)
N(1)	5527(5)	2162(8)	7005(9)
C(1)	4011(4)	5880(6)	7413(7)
C(2)	5355(5)	4657(7)	7570(7)
C(3)	6725(5)	5781(8)	8302(9)

2. Calorimetric Study

The crystals of 2-bromo-2-nitropropane-1,3-diol have been studied using a microcalorimeter of Calvet type in the temperature ranges 77–246 K and 305–419 K (the interval from 276 to 305 K has not been investigated in detail, but according to preliminary data, no phase transition occurs in this temperature range). The sample weight varies from 0.03 to 0.3 g. The cooling rate from room temperature to 77 K is approximately $3^\circ\,\mathrm{min}^{-1}$. The thermal properties of the substance are recorded on thermograms only when it is heated at the rate of $0.1^\circ\,\mathrm{min}^{-1}$. As the results show, no thermal effects have been observed in the temperature range 305–410 K. Figure 6 demonstrates calorimetric thermograms of crystal **I** in the high-temperature region, 305–415 K. The solid curve refers to the first step of heating, from 305 K to T^*, just after the latter phase was synthesized. In this temperature region three thermal effects have been observed: a single exothermic one ($Q = +0.173\,\mathrm{kcal}\cdot\mathrm{mol}^{-1}$) with center 349.5 K, and two endothermic ones with centers 354.5 K ($Q = -0.147\,\mathrm{kcal}\cdot\mathrm{mol}^{-1}$) and 374.0 K ($Q = -6.5\,\mathrm{kcal}\cdot\mathrm{mol}^{-1}$). After the sample is cooled from T^* to room temperature and then repeatedly heated to T^* (Fig. 6, dashed curve), the first two thermal effects disappear, in contrast to the thermal effect at 374 K, which is permanently reproduced. It follows that immediately after synthesis, the crystals exist in a metastable state which changes, to an equilibrium (or quasi-equilibrium) state on the very first heating. The reproducible peak at 374 K should be referred to as the first order crystal–crystal phase transition with temperature 362 K when heat release becomes noticeable (according to the sensitivity of the method), which may manifest the start of the phase transition and the emergence of the prephase state. It should be noted that in compound **II**, crystals of the first two metastable states have also been observed, but they have smaller heat effects than those of compound **I**. The thermal effect of the phase transition ($T_k = 372\,\mathrm{K}$) in crystal **II** is $6.71\,\mathrm{kcal}\cdot\mathrm{mol}^{-1}$ and is in good agreement with that of crystal **I** within the limits of accuracy. One should note that in crystal **II** the first two peaks have also been registered but have demonstrated a smaller thermal effect than that in compound **I**. The phase transition temperature, T_k, has been found to be 2° lower and has reached 372 K. At the same time, the temperature of the noticeable thermal effect of the prephase state appears to be roughly 365 K. The thermal effect of the transition is $6.71\,\mathrm{kcal}\cdot\mathrm{mol}^{-1}$ ($\pm 5\%$) and is compared with that of crystal **I**.

After further heating of substance **I** above T^* (dashed-and-dotted line), melting of the crystals starts with an endothermic effect at 387 K and is accompanied by a strong exothermic effect reaching $+69.0\,\mathrm{kcal}\cdot\mathrm{mol}^{-1}$. It may be referred to as an exothermic decomposition reaction in the course of melting of the substance. After the decomposition reaction stopped and the sample was cooled to room temperature, heating was repeated and showed no thermal effects in the temperature range 305–419 K. This fact has demonstrated a total conversion of the initial substance into products consisting of brown-black material resembling tar and partially dissolving in ethanol.

TABLE 3
Atomic Coordinates ($\times 10^4$) in the Structure II

Atom	*X*	*Y*	*Z*
Br(1)	8966(2)	999(2)	6928(2)
O(1)	6641(42)	3816(39)	4614(29)
O(2)	7609(29)	4077(22)	7524(32)
O(3)	8989(32)	3301(20)	3384(27)
O(4)	10236(43)	1494(33)	4117(35)
N(1)	9218(25)	2416(23)	4287(25)
C(1)	6423(37)	2305(26)	5291(28)
C(2)	8295(28)	2413(20)	5644(28)
C(3)	8565(39)	3900(31)	6329(37)

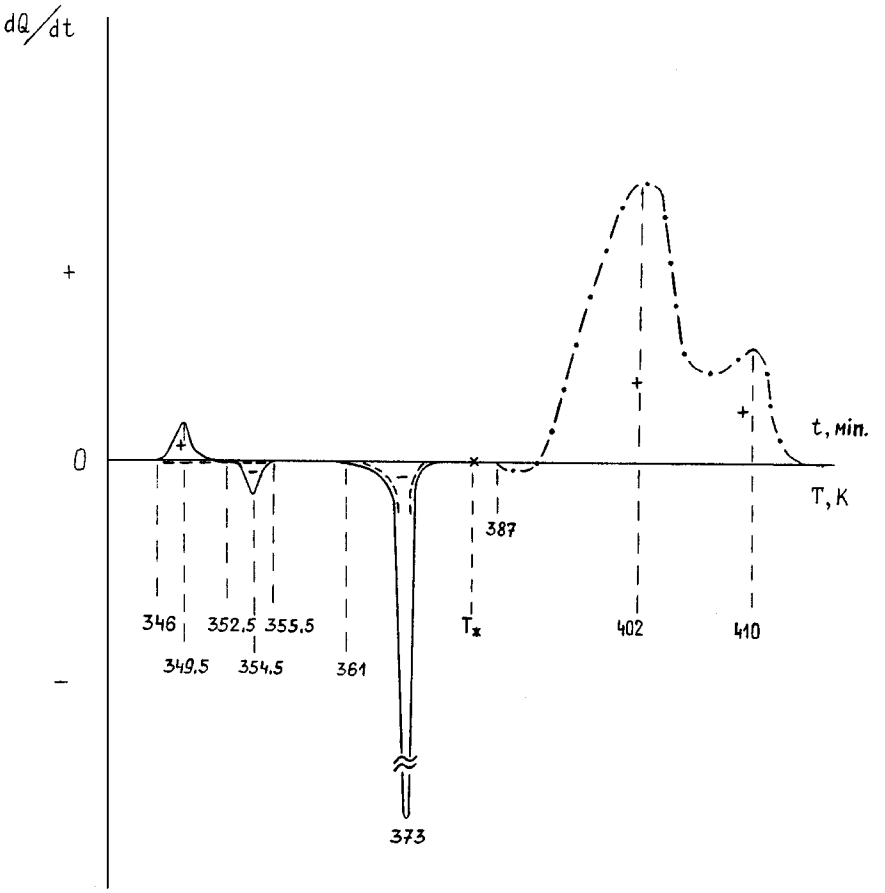

FIG. 6. Thermograms of crystal **I** in the region 305–405 K: solid line represents the first-step heating in the region from 305 K to T* after the synthesis; dashed line represents repeated heating to T* after cooling to room temperature; dashes and dots represent heating to temperature above T*.

3. Thermal X-ray Study of Crystals of 2-bromo-2-nitro-propane-1,3-diol

Temperature studies of the single crystal structure near the phase transition point have to explain, first, how the unit cell parameters change with temperature for crystal **I** (Table 5) and, second, what is going on in the molecule itself as temperature rises to the phase transition point.

We must note that the unit cell of crystal **I** has an anisotropic change: the parameter a in the chosen temperature interval grows by 0.3%, the parameter b by 1%, and the parameter c by 0.7%. This may be explained by the presence of limitless H-bonds with orientation approximately along the diagonal ac. The X-ray study has been conducted on a single crystal **I** at 343 K (as the higher temperature causes destruction of the crystal.

Crystallographic data of the structure $C_3H_6BrNO_4$ at $T = 343$ K (**I**–343) show that crystals of **I**–343 are monoclinic; $a = 8.026(2)$ Å, $b = 9.646(2)$ Å, $c = 8.960(2)$ Å, $\beta = 91.04(2)^\circ$, $V = 693.6(3)$ Å^3, $d = 1.915$ g/cm^{-3}, $\lambda = 1.5418$, Mu $= 7.76$ mm^{-1}; space group Cc, $z = 4$, $M = 200.0$, reflection number 368, $R = 0.052$. The atomic coordinates of the structure **I**–343 are shown in Table 6. The calculations of structures **I**, **II**, and **I**–343 were independent, so the coordinate origin does not coincide for all three structures. The disorder in the position of oxygen atoms O(1) and O(11) is

TABLE 5
Changes of the Unit Cell Parameters of Crystal I Caused by Elevation of Temperature

	T(K)				
Unit cell	193	263	273	333	348
a (Å)	7.992(2)	8.015(2)	8.026(2)	8.026(2)	8.016(2)
b (Å)	9.589(3)	9.631(3)	9.662(3)	9.664(3)	9.682(3)
c (Å)	8.920(2)	8.949(2)	8.963(2)	8.960(2)	8.987(2)
β (°)	90.75(3)	90.90(2)	91.00(2)	91.04(2)	91.23(2)

TABLE 6
Atomic Coordinates ($\times 10^4$) in the Structure I–343

Atom	*X*	*Y*	*Z*
Br(1)	7554(4)	− 1006(4)	7487(4)
O(1)	6266(53)	− 4161(69)	8056(49)
O(2)	10435(38)	− 1017(36)	10053(28)
O(3)	7883(68)	− 3040(59)	11289(58)
O(4)	6269(115)	− 1645(111)	10607(98)
O(11)	9575(250)	− 3845(101)	7428(153)
N(1)	7298(22)	− 2317(34)	10193(31)
C(1)	10182(33)	− 2297(41)	9319(34)
C(2)	8261(30)	− 2419(36)	8833(30)
C(3)	7982(29)	− 3783(41)	8091(26)

TABLE 7
Debye Powder Pattern of Polycrystal I at $T = 375$ K

HKL	2Θ	sin Θ	*d*	*a*
110 w.	12.40	0.1080	7.129	10.08
200 m.	17.40	0.1513	5.089	10.17
112 w.	21.32	0.1848	4.166	10.20
220 w.	26.50	0.2292	3.359	9.50
310 v.s.	31.12	0.2680	2.873	9.09
040 s.	36.17	0.3104	2.480	9.92
240 m.	42.83	0.3652	2.110	9.43

found in one of the –C–OH groups. Along with the main antiperiplanar arrangement of the C–O and C–C bonds, in which the population of the oxygen atom position is 0.7, a synclinic arrangement of the same bonds, in which the population of the oxygen atom position is 0.3, is found.

The change in the conformation of a definite number of molecules must be followed by the rupture of H-bonds inherent in structure **I** and the formation of new H-bonds inherent in structure **II**. We have also found great thermal oscillations of the –OH group oxygen atoms and the nitro-group oxygen atoms. Most probably, the molecule conformation change on temperature elevation begins from the torsion oscillation of a nitro group around the C–N bond. The oxygen atoms of the nitro group are positioned in one plane alongside the bromine atom and connected with it by orbital interaction (8). The energy of such attracting interactions is not high (approximately $3\,\text{kcal}\cdot\text{mol}^{-1}$). However, the beginning of torsional vibrations of the nitro group is interfered with not only by its interaction with the haloid atom, but also by steric hindrances between the oxygen atoms of the nitro group and the C–OH bonds arranged in an antiperiplanar way. The change in molecular conformation suggests overcoming not only of an intramolecular barrier (orbital interactions and steric hindrances) but also of an intermolecular interaction commensurable in energy (the energy of the intermolecular hydrogen bonds is about $6\,\text{kcal}\cdot\text{mol}^{-1}$). The results of the experiments have showed that when molecules change their conformation in the prephase state the start of the transition appears to be torsional vibrations of the nitro-group, which cause molecule conformation **I** to begin transforming into the more twisted and energetically more favorable conformation **II**.

Further investigations have been conducted with polycrystals and have dealt with the kinetics of prephase state accumulation. The theoretical Debye powder patterns based on the investigation of crystal structures **I** and **II** have previously been calculated. The calculations showed almost complete coincidence of the diffraction lines by 2Θ but different intensity values. To study the kinetics of the prephase state accumulation on the basis of Debye powder patterns, three separable reflections have been chosen, different in intensities in both the structures: (200), (110), (040). To identify the final state of the transition, the Debye powder pattern at $T = 375$ K has been obtained after the phase transition was completed. The final state can be represented mainly by the peaks identified in Table 7. The indexed peaks correspond to the body-centered cubic lattice (BCC) with cube edge $a = 9.77$ Å. Thus, the final state is a body-centered cube made of spheroids (balls having no strict spherical symmetry; see *a* dispersion) consisting of rotating molecules. In the initial crystals of space group *Cc*, the center of gravity of the molecule is still located in the body-centered cubic positions (unit cell parameters have close similarity: almost all the angles equal 90°). That is why, for the phase transition, no linear displacements of molecules are necessary and their rotation is sufficient. Note that the diffraction patterns will be the same in the case of the rotating molecules and in the case of the molecules statistically disoriented in the volume of the sphere.

4. Optic Microscopy Observations

The phase transition from anisotropic into isotropic structure (cubic) has been run in transparent crystals **I** and **II** at about 373 K. It was examined in a hot stage under an optical microscope in polarized light. The initial crystals of the substance look colorless, highly defective, and optically active (monoclinic phase) with transparent crystals 5–7 mm long and up to 0.5 mm thick. The crystals were introduced into the sample chamber of the hot stage (in close vicinity to the thermocouple gauge) between cover glasses. The accuracy of temperature control was $\pm 0.5°$. The account of the picture observed describing the behavior of the crystals during heating and cooling is presented below; microphotography could not be performed because of a sublimated material deposited on both cover glasses, which prevented good picture production.

The first temperature rise. The rate of heating was $5^\circ \cdot \text{min}^{-1}$. No changes in the crystals were noticed up to 348 K. At that temperature, a layer of sublimated material in the form of droplets (10–30 μm in diameter) was deposited on the upper cover glass. At 375 K, a phase transition into cubic lattice occurred. The first nuclei of the new phase appeared in two different places of the crystal, followed by a loss of optical activity. After the coalescence of some nuclei, the quantity of the cubic phase began to grow due to the advance of a transition front through the crystal. The boundary between the two phases presented itself as a prolonged zone about 10 μm wide. After the phase transition, the temperature increased to 383 K and then a slow cooling began.

The temperature fall. In the interval 383–355 K, the system underwent no change from the optically inert state. At 355 K a phase transition (or crystallization) was seen in the sublimated layer on the cover glass, and the layer transformed into a polycrystal film containing optically active crystals with dimensions 10–20 μm. The initial crystals stayed in the cubic phase up to 333 K, when a fast phase transition into optically active lattice took place. A further temperature decrease did not change the picture. After cooling to 313 K, another step of heating was performed.

Repeated heating and cooling. The initial crystals retained an invariable state (optical activity) up to 375 K, when the phase transition into cubic lattice occurred. The crystals in the layer on the upper cover glass underwent a phase transition (melting) only at 385 K (loss of optical activity). Thereafter, a liquid phase started forming; it appeared later on the crystals of the main substance. (A liquid phase can appear as a consequence of premelting of eutectics of the main substance, with the products of thermal decomposition likely to be tar-like products or polymers.) Total melting of all crystals both of the main substance and of the sublimated layer on the cover glass took place at 390 K. The temperature was then elevated to 408 K, maintained for 15 min, and then cooling was started again. All components of the system stayed molted up to 363 K, at which point they almost simultaneously crystallized into a cubic phase; at 343 K the phase transition occurred into an optically active state (monoclinic phase).

Thus the optic observations have shown that:

(a) 2-bromo-2-nitropropane-1,3-diol crystals undergo phase transition from an anisotropic (monoclinic) into a cubic phase at about 375 K;

(b) the influence of the prolonged heat may cause the formation of decomposition products and their interaction with the main substance; and

(c) a considerable overcooling is possible (reaching tens of degrees) at a temperature change in the region of phase transition.

5. Changes of Crystal Structure in the Prephase State and the Kinetics of Prephase Accumulation

During the temperature change of a crystal, particularly approaching the phase transition point, X-ray (X-ray phase) analysis permits the change in the reflecting planes of the initial crystal structure to be traced and a conclusion as to the structural reorganization in the prephase state to be made. With that, it seems worthwhile to carry on observations not only of the initial structure but also of the reflections indicating a new phase, as one might expect that the new phase nuclei can incept even before the phase transition temperature. In general, the initial crystal structure changes will not proceed simultaneously in all reflecting planes because of their nonequivalency due to the vicinity and buildup.

The changes in the intensity of reflection from certain planes may also be connected with recapture of the fall in intensity of the initial reflection by planes with growing reflection intensity (within the same initial crystal system). In other words, the temperature reconstruction of the initial phase molecules leads to a redistribution of electron density (and reflection intensity) from some reflecting layers to others and plays an important part in the new phase formation. Changes of this kind in the distribution of electron density are reversible but it is exactly they that define the prephase state. The appearance of new peaks connected with the formation of new phase nuclei exhibits intensity hysteresis of the reflections, depending on the temperature during the reversed temperature movement, because of considerable overcooling. This may help to distinguish between the prephase state and the earlier nucleation of a new crystal phase.

Taking the above into account, we offer experimental data of intensity change kinetics for some reflections of monoclinic phase **I** depending on the temperature near the point of transition into a cubic phase. The study has been conducted on powders introduced in the temperature cell of a diffractometer (temperature accuracy $\pm 2^\circ$). The intensity change registration vs time has been performed for two reflections of monoclinic phase **I**, (110) and (200), and one reflection of monoclinic phase **II**, (040), alongwith the reflection (040) of the cubic phase during phase transition. The selection of the reflections was determined by the fact that these base reflections with low indicies have been exhibited on diagrams with no additional interfering peaks. The integral intensities of the reflections have been normalized by an internal standard, reflection (002) of hexagonal boron nitride (separately for each experiment). Relative intensities of the reflections have been determined for all time–temperature points (Tables 8 and 9). Figure 7 demonstrates the kinetics of the intensity change of reflection (110). The curves for the three temperatures have a general character. Each curve shows first a fast fall with an almost constant

TABLE 8
Intensity Change $I/I(0)$ of the Reflections (110) and (200)

Time (min.)	Temperature (K)		
	348	358	365
	Reflection (110)		
0	1	1	1
15	0.918	0.885	0.851
32		0.772	0.707
41	0.800		
59		0.712	
62			0.527
70	0.800		
103		0.712	
108	0.787		
111			0.520
149		0.721	
	Reflection (200)		
0	1	1	1
18			0.743
19	0.847	0.816	
30		0.678	0.475
46	0.806		
63		0.675	
68			0.325
74	0.823		
108		0.616	
112	0.812		
118			0.228
152		0.587	

Note. I represents the intensity of the reflection in the current experiment; $I(0)$ represents the intensity of the normalizing peak of boron nitride (002).

TABLE 9
Intensity Change $I/I(0)$ of the Reflections (040) MII and (040) C

Time (min.)	Temperature (K)		
	348	358	365
	Reflection (040)M**II**		
0	0.050	0.110	0.175
15	0.075	0.254	0.272
27	0.150	0.293	
29			0.310
57	0.275	0.335	
62	0.280		0.280
102	0.340	0.311	0.250
114			0.225
148	0.340	0.210	0.102
	Reflection (040)C		
0	0	0	0
15	0	0.050	0.075
27	0	0.125	0.135
29	0		
57	0	0.198	
62	0		0.285
102	0	0.268	0.465
114	0		0.515
148	0	0.435	
	Reflection (040)C in the cubic phase at 378 K		
			0.940

Note. I represents the intensity of the reflection in the current experiment; $I(0)$ represents the intensity of the normalizing peak of boron nitride (002).

rate. The fall passes to a zero-rate section, the position of which depends on the experiment temperature. The picture is determined by the electron density change in the reflecting planes, probably because of the liberation of the hydrogen bond R–OH---HO–R between neighboring molecules and the increase in thermal vibration. The number of liberated molecules grows with temperature, but an equilibrium is attained between the initial molecules and the liberated ones. Thus one may write

$$(N_i - N_*)\,\frac{k_{(1)}^{(hkl)}}{k_{(-1)}^{(hkl)}}\,Ne_* \qquad [1]$$

where N_i is the number of initial molecules; Ne_*, the number of liberated molecules at equilibrium set; $k_{(1)}^{(hkl)}$, the Arrhenius' constant for the direct reaction; and $k_{(-1)}^{(hkl)}$, the Arrhenius' constant for the reversed reaction. Then one may write for the equilibrium (9):

$$k_{(1)}^{(110)}\cdot(N_i - Ne_*) = k_{(-1)}^{(110)}\cdot Ne_* \text{ or } k_{(1)}^{(110)}\cdot(1-f) = k_{(-1)}^{(110)}\cdot f, \qquad [2]$$

where $f = Ne_*/N_i$, the fraction of the transition (depth of the reaction), and

$$k_{(1)}^{(110)}/k_{(-1)}^{(110)} = f/(1-f). \qquad [3]$$

In the experiment, the direct reaction rate (for the initial rate of the intensity fall) and the value of $f/(1-f)$ (for the equilibrium set) have been measured. The values of the kinetic parameters of the direct reaction constant have been calculated graphically and by PC processing. For $k_{(1)}^{(110)}$ the expression

$$k_{(1)}^{(110)} = 1.2\times10^2\cdot\exp(-9800/RT) \qquad [4]$$

has been obtained.

The reversed reaction constant has been calculated in the same way: Arrhenius' graph was processed by least squares method, then the constant was evaluated as $k_{(-1)}^{(110)} = 6.8\times10^{-11}\cdot\exp(10{,}800/RT)$. Thus the equilibrium constant

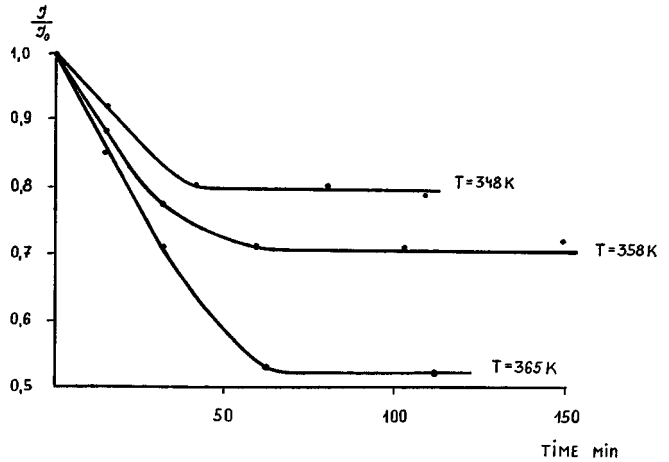

FIG. 7. Kinetics of the intensity decrease of reflection (110).

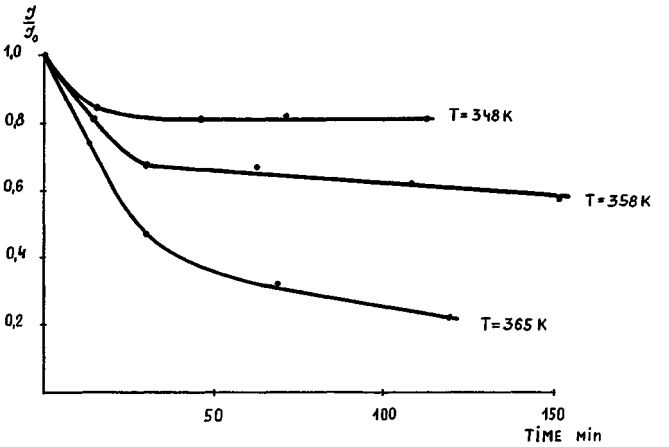

FIG. 8. Kinetics of the intensity decrease of reflection (200).

equals

$$k_{(e)}^{(110)} = k_{(1)}^{(110)}/k_{(-1)}^{(110)} = 1.34 \times 10^{12} \cdot \exp(-20{,}400/RT). \quad [5]$$

The results show that in reflection (110) a number of molecules stay in the initial state (until the transition into a cubic lattice occurs), trying to "save" the monoclinic lattice. The picture of the intensity change of reflection (200) is somewhat different (Fig. 8). A quick initial intensity fall, which later begins to slow, has been observed. Figure 9 shows that no equilibrium is set for the experimental lag of time, and the reflection intensity (200) falls steadily. The evaluation of the initial rate constant gives

$$k_{(1)}^{(200)} = 2.07 \times 10^{4} \cdot \exp(-13{,}000/RT). \quad [6]$$

One can see from Fig. 9 that the temperature dependence of the slow stage of the intensity fall is stronger than that of the initial stage. The evaluation of the slow stage rate constant gives

$$k_{(S)}^{(200)} = 1.04 \times 10^{16} \cdot \exp(-34{,}400/RT). \quad [7]$$

The evaluation has been conducted with the assumption that the rate stays constant. $k_{(S)}^{(200)}$ probably does not manifest a simple process but includes the reverse reaction constant. The type of reflection intensity (200) slope points to the steady degradation of the reflecting layer structure associated with an electron density decrease.

The layer (040) attracts particular interest both in monoclinic and in cubic phases. The dynamics of its changes indicates that there are changes in the conformational and orientational states of the molecules. In monoclinic phase (**I**), the position of reflection (040)M**I** corresponds to the angle $2\Theta = 37.17$ and its intensity is very low (close to the background). In monoclinic phase (**II**), reflection (040)M**II** retains its position but has considerably greater intensity. The powder diffraction pattern obtained by calculation confirms the difference in intensity between these two peaks, (040)M**I** and (040)M**II**, with the same position ($2\Theta = 37.17$). In the cubic phase, reflection (040) C is positioned in the region of $2\Theta = 36.17$, where no other reflections of the monoclinic phase are present. This makes the reflection very useful for checking changes of the molecular state in the monoclinic phase. It may be said that the intensity changes of the reflection $2\Theta = 37.17$ point to the change of the molecular state featuring monoclinic phase **II**; at the same time, the intensity increase of reflection $2\Theta \approx 36.17$ relates to the formation of diffraction domains of the cubic phase and the beginning of molecular rotation. The normalization of the intensity of the reflection (040)M**II**, has been performed with the same internal standard as for the reflections (110) and (200). Figure 9 shows a rise in the relative intensity of the reflection (040)M**II** at 348 K. That is, a certain number (*N*e∗) of the molecules liberated from hydrogen bonds create regular formations of molecule (**II**∗), coinciding with the position of the existing layer of reflection (040)M**I** and increasing with its electron density. The reflection (040) C is not appreciable at this temperature. Thus one may conclude that at 348 K an intermediate phase **II**∗ has been formed in the prephase state. The structure of the intermediate phase is structurally close to that of phase **II** (obtained by low temperature synthesis); their difference consists only in slight disorientation of the molecules of the intermediate phase formed at a relatively high temperature. The relative intensity of the intermediate phase reflection (040)M**II**∗ grows rather quickly during the starting period; then a sharp drop occurs. At 358 K and 365 K, a rise in intensity

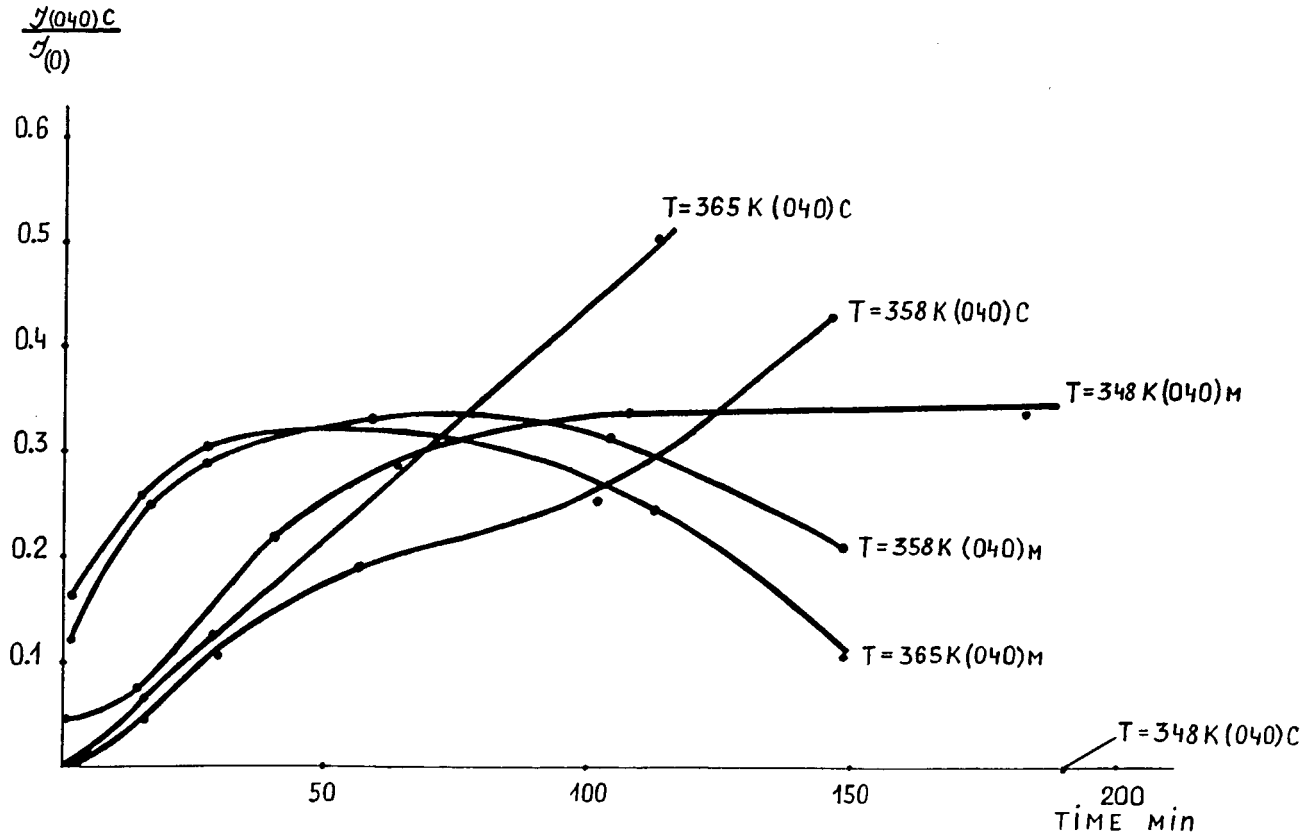

FIG. 9. Kinetics of the intensity change of reflections (040) M**II**∗ and (040) C.

of the reflection (040) C has been registered. The fast growth of the reflection intensity coincides with the decrease in intensity of the reflection (040)M**II**∗. This fact shows that the two processes run with different starting times. The situation evidences that:

(1) the beginning of the cubic phase formation occurs at a temperature below $T = 375$ K in the monoclinic phase;

(2) the rate of formation of reflecting layers (040) C starts growing rapidly only when a sufficient number of molecules are liberated from hydrogen bonds to generate blocks with adequate dimensions to produce diffraction; and

(3) the cubic phase formation proceeds through an intermediate phase, the monoclinic phase **II**∗.

The picture may explain the induction period of the appearance of reflection (040) C inside the monoclinic phase, connected with the necessity of transformations in the reflecting layers and formation of domains of coherent scattering.

RESULTS AND DISCUSSION

The experimental data permit us to elucidate clearly the processes in the crystal lattice of 2-bromo-2-nitropropane-1,3-diol leading to prephase state formation and its particularities. During the heating of crystal **I**, weakening and rupture of the intermolecular hydrogen bonds occur, resulting in the liberation of the molecules and their acquisition of a twisted shape and a favorable configuration. Below the phase transition temperature, the process is reversible, and in crystal **I** a certain concentration of such "activated" molecules exists in dynamic equilibrium with the molecules of the initial lattice. Thus molecules in the "activated" state may migrate through the crystal. With the rise in temperature, the concentration of the "activated" molecules reaches the critical value when the formation of intermediate-phase nuclei—the domains of coherent scattering (retaining monoclinic phase)—becomes possible. The reverse reaction makes the critical concentration slightly dependent on temperature. The formation of coherent scattering domains in the intermediate phase is also confirmed by the intensity rise of the reflection (040)M**II**∗.

The "activated" (liberated) molecules may feature an intensification of torsion oscillations and, later, nitro-group rotation around the C–N bond. Beginning with a certain scale for the coherent scattering domains of the intermediate

phase, the molecules in the domains acquiring total rotation (with temperature rise), and a monoclinic symmetry converts into a cubic one. Since the transition takes place only in sufficiently large domains of the intermediate phase, nuclei in the cubic phase appear in the bulk of the monoclinic phase at temperatures below the phase transition point. It should be emphasized that the quantity of the intermediate phase depends slightly on temperature. The formation of the cubic phase nuclei is also proved by the corresponding peaks on the diffractogram (however, it is difficult to sort them out separately due to strong overlap in the reflections of the initial phase). At the temperature drop, the value of the reflection(040)M**II**∗ returns to the starting magnitude and the value of reflection (040) C (cubic nuclei inside the monoclinic crystal) retains its intensity for some time, demonstrating pronounced hysteresis. A continuous temperature rise produces a real phase transition in which all molecules start rotating, creating a spheroidal volumes of electron density and thus crystal transfers into a cubic phase. The process may be presented diagrammatically. If we designate

M—the molecule of 2-bromo-2-nitropropage-1,3-diol,

$\langle M \rangle$—M in the monoclinic lattice,

M∗—the "activated" (liberated) molecules,

$\langle M* \rangle$—the activated molecules in the monoclinic lattice,

(M∗)—the coherent scattering domain formed of the M* molecules, the intermediate phase domains.

$\langle (M*) \rangle$—(M∗) in the monoclinic lattice, the intermediate phase in the monoclinic lattice,

∗M∗—the rotating molecule (as a rotating toto),

(∗M∗)—the coherent scattering domain formed of ∗M∗,

$\langle (*M*) \rangle$—(∗M∗) in the monoclinic lattice (nuclei of cubic phase in the monoclinic one), and

[∗M∗]—the cubic lattice formed of rotating molecules above the phase transition point,

then the process in crystal during the temperature rise may be presented as follows:

$\langle M \rangle \rightleftarrows M* \rightleftarrows \langle (M*) \rangle$	$\longrightarrow \langle (*M*) \rangle$	$\longrightarrow$	[∗M∗]
reversible stages of the prephase state	hysteresis stage prephase state	real phase transition	new phase
the processes determining the prephase state in the monoclinic lattice in dependence on temperature		T phase transition	new cubic lattice

$\longrightarrow$ temperature $\longrightarrow$ T phase transition $\longrightarrow$

As has already been remarked, two components take part in the formation of the prephase state: reversible and hysteretic. Their part depends on the crystal temperature. The concentration $\langle (M*) \rangle$ has a slight dependence on temperature, probably because of two controlling mechanisms:

(1) the transfer to the state $\langle (*M*) \rangle$ after the coherent scattering domains $\langle (M*) \rangle$ reach critical dimensions to form $\langle (*M*) \rangle$; and

(2) the disintegration of $\langle (M*) \rangle$ to separate molecules M∗. The study shows that in the preparation of the prephase state, the crystals may suffer an essential structural reconstruction and the processes must be most pronounced in the "multiforce" crystal lattice consisting of complex molecules as, for example, in 2-bromo-2-nitropropan-1,3-diol.

The analysis of the prephase state may prove useful in many cases, such as the study of aging of compounds and the investigation of mechanisms of thermal decomposition of substances. The present study shows that in these cases the real structure of crystal lattice at the decomposition temperature may essentially differ from the structure of the same substance determined by X-ray methods at room temperature. This fact has to be taken into account in examination of the detailed mechanism of the process.

ACKNOWLEDGMENT

This work was supported by the Russian Foundation for Basic Research (Grant 97–03–32605 a).

REFERENCES

1. E. Schmidt and R. Wilkendorf, *Chem. Ber*. **52,** 309 (1919).
2. B. S. Fedorov, N. I. Golovina, V. V. Arakcheeva, R. F. Trofimova, and L. O. Atovmyan, *Izv. Ross. Akad. Nauk*, *Ser. Khim.* (5), 1217 (1996).
3. I. G. Gusakovskaya and T. I. Larkina, *Fiz. Tverd. Tela.* **15**(5), 1329 (1973).
4. A. R. Ubbelohde, *Trans. Faraday Soc*. **34**(2), 292 (1938).
5. N. I. Golovina, L. O. Atovmyan, N. V. Chukanov, G. V. Oreshko, R. F. Trofimova, M. A. Fadeev and L. T. Eremenko, *Zh. Strukt. Khim.* **31**(1), 126 (1990).
6. N. I. Golovina, A. N. Titkov, A. V. Raevskii, and L. O. Atovmyan, *J. Solid State Chem.* **113**(2), 229 (1994).
7. D. S. S. Gowda and R. Rudman, *J. Chem. Phys.* **77**, 4666 (1982).
8. B. S. Fedorov, N. I. Golovina, L. S. Barinova, V. V. Arakcheeva, R. F. Trofimova, and L. O. Atovmyan, *Izv. Akad. Nauk*, *SSSR Ser. Khim.* (10), 2372 (1991).
9. H. E. Avery, "Basic Reaction Kinetics and Mechanisms", p. 33. Macmillan, New York, 1974.